Effect of Ligand Aromaticity on Cyclohexane and Benzene Sorption in IRMOFs: A Computational Study

Kevin Dedecker, Martin Drobek, Anne Julbe

▶ **To cite this version:**

Kevin Dedecker, Martin Drobek, Anne Julbe. Effect of Ligand Aromaticity on Cyclohexane and Benzene Sorption in IRMOFs: A Computational Study. Journal of Physical Chemistry B, 2023, 127 (51), pp.11091-11099. 10.1021/acs.jpcb.3c06886 . hal-04625347

HAL Id: hal-04625347
https://hal.science/hal-04625347

Submitted on 26 Jun 2024

HAL is a multi-disciplinary open access archive for the deposit and dissemination of scientific research documents, whether they are published or not. The documents may come from teaching and research institutions in France or abroad, or from public or private research centers.

L'archive ouverte pluridisciplinaire **HAL**, est destinée au dépôt et à la diffusion de documents scientifiques de niveau recherche, publiés ou non, émanant des établissements d'enseignement et de recherche français ou étrangers, des laboratoires publics ou privés.

Effect of Ligand Aromaticity on Cyclohexane and Benzene Sorption in IRMOFs: A Computational Study

Kevin Dedecker, Martin Drobek, Anne Julbe*

Institut Européen des Membranes (IEM); CNRS, ENSCM, Univ Montpellier; Place Eugène Bataillon; 34095 Montpellier; France

KEYWORDS: Metal Organic Framework, IRMOF, pyrene, sorption, benzene, cyclohexane, aromatics, volatile organic compounds

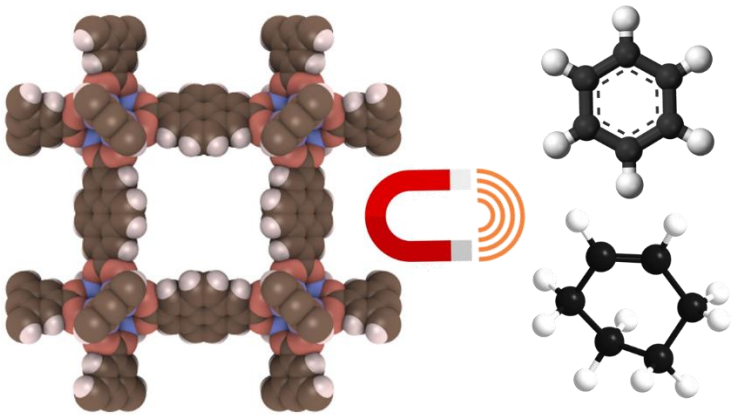

TOC Graphic

Abstract

A series of four isoreticular MOFs (IRMOF-1, -10, -14 and -16) was selected for a computational investigation of the effect of ligand aromaticity on the adsorption capacity of an aromatic VOC (benzene) compared to its non-aromatic analogue (cyclohexane). The affinity of the adsorbates was evaluated by calculating Henry's constants and adsorption enthalpies. It has been evidenced that while K_H values decrease with ligand elongation (IRMOF-10 and -16), inserting a pyrene core into the MOF structure (IRMOF-14) increases both the cyclohexane and benzene adsorption efficiency by ~290 and 54% respectively. To elucidate host-guest interactions, we sought to locate preferential adsorption sites in MOF structures for the two VOCs studied using the GCMC method. It appears that benzene interacts with the metal center (Zn_4O clusters) and most of the ligand, while cyclohexane tends to localize preferentially only near the Zn_4O clusters. Co-adsorption isotherms (equimolar mixture of benzene and cyclohexane) demonstrated the preferential adsorption of cyclohexane due to the stronger affinity with the MOF structure. On the other hand, for other isoreticular structures, the ligand elongation leads to a shift of the adsorption curve of cyclohexane caused by pore size increase and therefore, less interactions with the walls. This phenomenon is counterbalanced in the case of IRMOF-14 due to stronger interactions between cyclohexane and pyrene groups. The present results thus open perspectives in the design of promising MOF candidates for high-performing separation, sorption/detection of hydrocarbon VOCs.

Introduction

The deterioration of air quality is more than ever a major concern due to the increasing emissions of harmful gases and vapors in the environment (e.g. hydrocarbons, aldehydes, NO_x, SO_x, H_2S, O_3). Some of them, classified as volatile organic compounds (VOCs) are currently the subject of

particular attention from health organizations because of their harmful effects on the integrity of the human population[1–7]. In this context, the deleterious effects of benzene which can lead to fatal diseases such as anemia and leukemia[8–11] are often discussed. Consequently, tolerated individual exposure is officially regulated and reduced from year to year to reach a benzene concentration limit of less than 1 ppm[12]. The management of benzene contamination therefore remains highly challenging due to its omnipresence in urban areas and particularly in confined spaces (e.g. homes, workplaces) where the concentration can often reach 1.5 times the outdoor street level[13]. Despite its lower detrimental effects on human health, cyclohexane is known to have pernicious effects on the brain including headaches, sleepiness, dizziness, verbal memory impairment and oxidative stress[14].

To protect individuals, an appropriate solution relies on a combination of air purification/monitoring using effective adsorbents for the exclusive capture and detection of benzene and/or cyclohexane. The traditional materials available such as activated carbons[15], or zeolites[16], generally suffer from a lack of selectivity in the presence of humidity. Thus, despite their affordability and availability in the market, they still remain problematic candidates for their practical use in atmospheric conditions[17,18].

Furthermore, benzene and cyclohexane form an azeotropic mixture which is challenging to separate due to their similar boiling points (80.1 and 80.7°C for benzene and cyclohexane respectively)[19]. This is of great importance especially because 85% of cyclohexane is produced industrially through catalytic hydrogenation of benzene[19,20].

In order to overcome this drawback, a large research activity is now focused on the development of other adsorbent materials such as Metal-Organic Frameworks (MOFs) representing a subclass of coordination polymers known for their rich structural diversity and their versatile properties[21].

They result from the self-assembly of metallic clusters connected by organic linkers to form periodic structures generally exhibiting both high pore volume and high specific surface area[22]. Beyond their impressive porosity, their adsorption properties can also be finely tuned thanks to a judicious choice of metals and ligands. Therefore, MOFs have been intensely studied for efficient capture of VOCs[23]. For example, in a previous study we demonstrated that $[Pd(2\text{-pymo})_2]_n$ is able to preferentially adsorb benzene rather than n-hexane, cyclohexane and toluene while its isostructural analogue, $[Cu(2\text{-pymo})_2]_n$ interacts more strongly with n-hexane[24]. This research work underlines the significant contribution of palladium for the preferential adsorption of benzene and highlights the potential of Pd-based MOFs for the selective capture of aromatics. Furthermore, as evidenced previously, functionalization of the ligand can also significantly modify the sorption properties of MOFs[25–27]. For instance, UiO-66-$(CF_3)_2$ bearing perfluorinated groups on terephthalate ligands, exhibits higher hydrophobicity than its isostructural parent (UiO-66(Zr)) and concomitantly interacts strongly with different VOCs[25] making this MOF greatly interesting for their selective capture in humid conditions[26,27]. Finally, thanks to the fine adjustment of the length of the ligand, one can also precisely control the size of pore aperture inducing either molecular sieving[28] or/and host-guest interactions enhanced by the confinement effect[26].

Compared to these aforementioned widely studied tunable characteristics, the impact of ligand aromaticity is rarely explored parameter in literature for VOC removal by MOFs[29,30]. Yet, this specific feature could represent an easy and accessible way to enhance interactions with hydrocarbons (e.g. alkanes, aromatics) due to the vast panoply of polyaromatic ligands commercially available instead of synthesizing complex ligands. Indeed, modifying the number of phenyl rings and their arrangement (fused or separated cycles) can lead to adjusting the sorption properties and ultimately to increasing the affinity of hydrocarbons for MOFs such as alkanes or

aromatics. This has been briefly demonstrated for SION-82, a pyrene-containing MOF, which exhibits strong π-π interactions with aromatic molecules such as pyridine, thiophene and benzene[29]. Similarly, BUT-57[30] exhibits higher benzene uptake than common MOFs (e.g. MIL-101(Cr), ZIF-8, HKUST-1). However, it should be underlined that examples and comparisons of performance between isoreticular structures potentially highlighting the positive effects and advantages of ligands containing pyrene are still very scarcely described in the literature.

With this in mind, in the present computational study, we aim to highlight the impact of the aromaticity of the ligand of IRMOFs on the efficiency of adsorption for the separation of benzene and cyclohexane. The IRMOF family was chosen, taking advantage of a large variety of its reported isoreticular structures with elongated but also polyconjugated ligands[31]. Additionally, IRMOF-1 has also been studied for the adsorption/separation of cyclohexane/benzene[32], making comparisons with experimental data feasible. Demonstration of the significant impact of pyrene-containing ligands on the sorption properties of MOFs would boost the potential applications of other MOFs in high-performing devices for selective adsorption, detection or membrane separation. To this end, we explored four well-known isoreticular MOFs, different in the aromaticity of their ligands (IRMOF-1: benzenedicarboxylate, IRMOF-10: biphenyl-4,4'-dicarboxylate, IRMOF-16: [p-terphenyl]-4,4"-dicarboxylate and IRMOF-14: pyrene-2,7-dicarboxylate) for the adsorption of pure benzene and its non-aromatic analogue (cyclohexane), as well as their selective separation from an equimolar mixture using the Grand Canonical Monte Carlo (GCMC) simulation.

Models

To mimic the adsorbate molecules, two distinct models were used: *i)* the explicit-hydrogen version of the transferable potentials model for phase equilibria (TraPPE-EH) developed by Siepmann et al. for benzene[33,34] and *ii)* that of Y. M. Muñoz-Muñoz et al. for cyclohexane[35], respectively.

Benzene molecules were composed of explicitly expressed carbon and hydrogen atoms while cyclohexane was treated as a ring of CH_2 beads connected to each other in a chair conformation (**Figure 1**). Both adsorbates were considered rigid. Even though at room temperature, cyclohexane can adopt five flexible conformations: chair, half-chair, boat, twisted-boat I and twisted-boat II[36], recent studies have shown that locking cyclohexane in the chair position provides an excellent approximation for GCMC simulation[35,37]. Indeed, the chair conformation has the lowest energy and the Boltzmann distribution shows that in vapor phase at 298K only 0.01% of twisted-boat conformation is present[37]. Hence, considering the rigid chair conformation at 298K to model cyclohexane is a reasonable approach for GCMC simulations. Non-bonded dispersive interactions were expressed using the Lennard-Jones (L-J) potential and force field parameters for benzene[33,34] and cyclohexane[35] were taken from the literature (**Table 1**). The model of benzene and cyclohexane molecules with bond lengths, angles and positions of pseudo-atoms C_benz (carbon in benzene), H_benz (hydrogen in benzene) and CH_2 (methylene groups in cyclohexane) pseudo atoms is given in Table S1. The coordinate system is orthogonal.

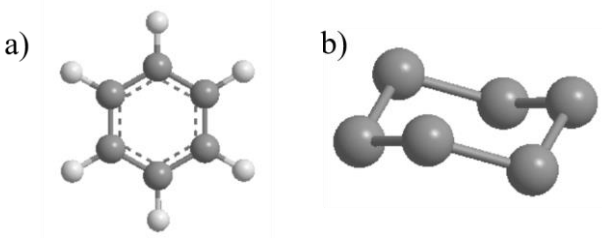

Figure 1. Illustration of the a) benzene and b) cyclohexane models used for the GCMC simulations.

Table 1. List of L-J potentials for benzene and cyclohexane.

Type	σ (Å)	ε/kB(K)	Charge
C_Ar[33,34]	3.55	35.24	-0.115
H_Ar[33,34]	2.42	15.03	0.115
CH_2_sp_3[35]	3.497	87.009	0.0

Four isoreticular cubic structures were selected: IRMOF-1, -10, -14 and -16, all belonging to the IRMOF series (**Figure 2**)[31]. They differ in the number of benzene rings composing the ligand and their arrangement. IRMOF-1 (also known as MOF-5) is composed of terephthalate ligands (BDC) linked to Zn_4O clusters forming a 3D structure composed of two different cavities (with diameters of 11 and 15 Å)[38]. Concerning IRMOF-10 and IRMOF-16, they are constructed from biphenyl-4,4'-dicarboxylate (BPDC) and [p-terphenyl]-4,4"-dicarboxylate (TPDC) ligands, respectively. IRMOF-14 formed from pyrene-2,7-dicarboxylate (PDC) ligands with four fused aromatic rings was selected as a candidate with higher π electron density. For GCMC simulation, IRMOF frameworks were fixed by crystallographic data derived from single-crystal X-ray diffraction and generated using Crystallographic Information Files (CIFs) from the CCDC database (filing numbers: IRMOF-1: 175572; IRMOF-10: 175580; IRMOF-14: 175583; IRMOF-16: 175584)[31]. L-J potentials modeling MOF-adsorbate interactions were extracted from Dreiding[39] and Universal Force Field (UFF)[40] and were combined using the Lorentz-Berthelot mixing rules (**Table 2**). The attribution of the atomic charge was taken from the literature since it was already calculated for the same IRMOF structures using the Density Functional Theory (DFT) method and validated for the adsorption of CO_2[41].

Table 2. List of L-J potentials for constituent atoms of IRMOF structures[39,40].

Type	Force Field	σ (Å)	ε/kB(K)
Zn	UFF[40]	2.46155	62.3992
C	Dreiding[39]	3.47299	47.8562
H	Dreiding[39]	2.84642	7.64893
O	Dreiding[39]	3.03315	48.1581

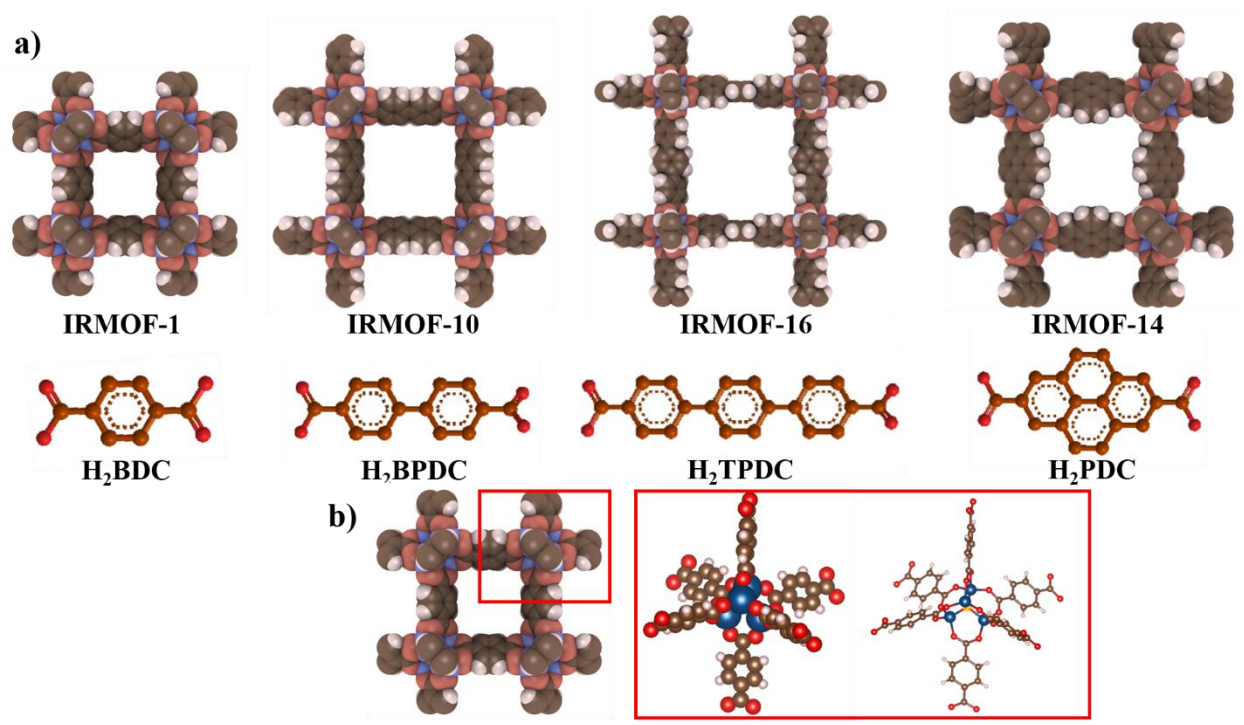

Figure 2. a) Illustration of the IRMOF structures studied and their respective ligands. Zinc: blue, carbon: brown, oxygen: red and hydrogen: white., b) Structure of the metal node for IRMOF-1.

Methods

RASPA software was used for all simulations. Co-adsorption isotherms for the IRMOF series were obtained for an equimolar mixture of benzene/cyclohexane (50:50) using the Grand-

Canonical Monte Carlo (GCMC) method at 298 K. The amount of each component was estimated at different pressures ranging from 0.1 to 1.0 kPa. The selected MOF structures were kept rigid and their respective supercells were constructed with a length at least twice the Van der Waals cutoff value and large enough to include both types of cavities. For both Coulomb and Van der Waals short-range interactions and in line with previous studies[42,43], a cutoff value of 12 Å was selected as an appropriate trade-off between computational cost and calculation accuracy for this type of simulations to account for all Lennard-Jones (LJ) interactions. It is to note that analytical tail corrections also were applied. Ewald summation with a relative accuracy of 10^{-6} has been applied for long-range electrostatic interactions. Accordingly, 2 x 2 x 2 supercells were considered for all systems. As already done in other studies[44,45], DFT has not been applied to minimize the crystal structure. GCMC simulations were carried out using 10,000 initialization cycles and 1,000,000 production cycles. Henry's constant (K_H) were obtained using Widom's insertion method for single-component systems. Their calculations were made by performing 200,000 production cycles without initialization cycles. For all GCMC simulations, the number of cycles was optimized to reach equilibrium (Figure S1-3). Enthalpy of adsorption (ΔH_{ads}) at low coverage were estimated using Van 't Hoff relation by plotting $\ln(K_H)$ vs 1/T for four temperatures (Figure S4,5). The values of K_H and ΔH_{ads} were considered to assess the affinity and adsorption strength of benzene and cyclohexane towards the studied MOF structures.

Results and discussion

Single-component adsorption

A first study was conducted to evaluate the affinity of cyclohexane and benzene with IRMOF structures. For this purpose, Henry's constants and adsorption enthalpies at 298 K were obtained by computation for the two adsorbates studied separately (**Table 3**). Actually, the K_H value is a

relevant indicator of adsorbate affinity at low pressures and can therefore shed light on the effect of ligand aromaticity on host-guest interactions. Surprisingly, when considering single gas adsorption, the results obtained for all the MOFs studied suggest that cyclohexane exhibits higher K_H and ΔH_{ads} values compared to benzene.

Table 3. Calculated K_H and ΔH_{ads} values with errors between parenthesis. The difference (Δ) with the IRMOF-1 values is expressed in %.

IRMOF	**K_H (mmol.10^{-4}/g/Pa)**				**ΔH_{ads} (kJ/mol)**			
	Cyclohexane		**Benzene**		**Cyclohexane**		**Benzene**	
	Value	Δ (%)	Value	Δ (%)	Value	Δ (%)	Value	Δ (%)
IRMOF-1	24.4 (0.1)	-	14.8 (0.1)	-	-33.2 (0.1)	-	-32.7 (0.2)	-
IRMOF-10	31.2 (0.5)	+28	7.1 (0.1)	-52	-35.7 (0.2)	-7.5	-30.9 (0.2)	+5.5
IRMOF-16	28.5 (0.4)	+17	6.0 (0.1)	-60	-36.0 (0.2)	-9.1	-31.2 (0.2)	+4.6
IRMOF-14	95.1 (0.5)	+290	22.8 (0.1)	+54	-38.6 (0.2)	-16.3	-34.0 (0.1)	-4.0

This phenomenon is explained by the nature of host-guest interactions[32]. Indeed, benzene has C-H···π donor/acceptor characteristics whereas cyclohexane is only donor. IRMOF-1 itself provides a C-H···π acceptor/donor environment. At low pressures, the adsorption of cyclohexane is favored over benzene due to its flexibility allowing more efficient accommodation of the cyclohexane molecule in the pore cavities of the MOF than rigid benzene. The preferential location of the

adsorbates was evidenced by their presence density obtained by computation after insertion of a single molecule of benzene or cyclohexane in the IRMOF-1 structure (**Figure 3**). For better visualization, a unit cell is shown with a density contour. It can be observed that benzene is located both near the Zn_4O metal node and the aromatic ring of the ligand. On the contrary, cyclohexane is only present near the metal node and seems to interact with the ligand to a significantly lesser extent. It should be noted that obtained of density contour are in a good agreement with the literature where DFT calculations have been performed to locate benzene and cyclohexane molecules in IRMOF-1 at low loading[32].

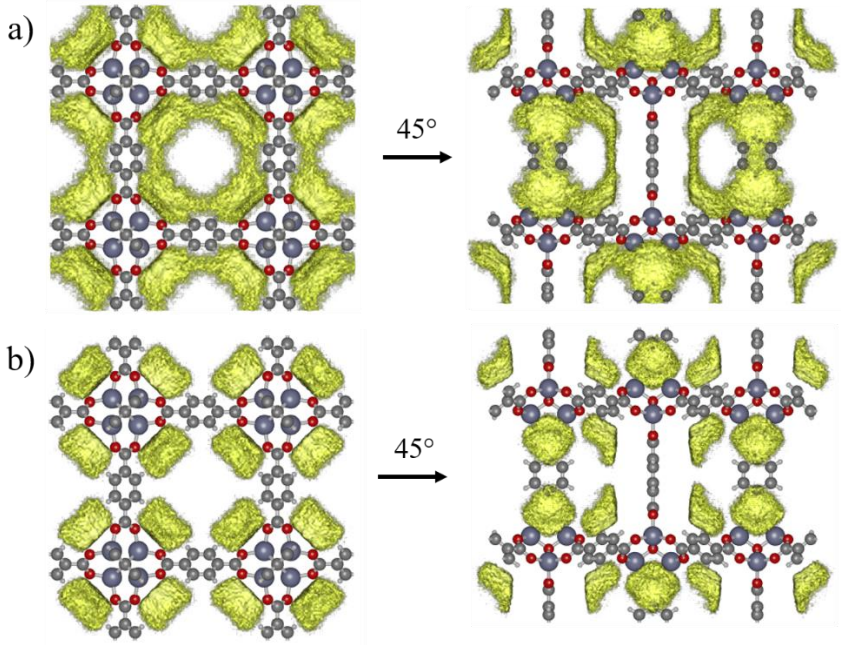

Figure 3. Density plots for a) benzene and b) cyclohexane in IRMOF-1 structures. Zinc: dark grey, carbon: light grey, oxygen: red and hydrogen: white.

Interestingly, K_H values decrease for longer ligands (i.e. BPDC and TPDC in IRMOF-10 and IRMOF-16 respectively) for benzene, indicating a loss of favorable interactions between the adsorbates and MOF structure (**Table 3**). A possible explanation may rely on the expansion of the unit cell, greatly reducing the number of interactions with the surrounding walls in the MOF

adsorbent. Additionally, BDC ligands (in IRMOF-1) differ from BPDC and TPDC ones in terms of aromaticity. Indeed, the addition of phenyl rings enriches the number of π electrons per ligand, which should normally promote π-π interactions with benzene. However, the steric hindrance induced by the hydrogen atoms located on the benzene rings leads to their rotation expressed by non-zero torsion angle. This loss of planarity reduces the delocalization of π electron and thus weakens π-type host-guest interactions. In addition, the loss of ligand planarity makes such adsorbate accommodation less efficient.

In this context, Y. Mo et al. elucidated the forces governing the stereochemistry of biphenyl[46]. They hypothesized that the torsion angle between the two rings is governed by two forces: the electron delocalization effect and steric repulsion favoring planar and perpendicular conformation, respectively. It has been shown that the stabilizing energy of each conformation is almost similar and therefore a torsion angle of 40° is a compromise between these opposing forces. They also conclude that π electrons are retained in each phenyl ring, thus the latter behave as independent benzene entities instead of pure conjugated systems. In the case of IRMOF-10 and -16, the torsion angle of BPDC and TPDC can be inferred from the MOF structure obtained from the Crystallographic Information Files (CIFs) (**Figure 4**). Interestingly, BPDC remains planar even when sterically constrained while TPDC exhibits a 45° torsion angle between each ring. Considering that the most stable conformation of biphenyl is twisted, it can be assumed that the planarity observed for BPDC is forced by structural constraints to preserve the cubic topology. These aforementioned structural constraints are also respected in the case of IRMOF-16 since the terminal phenyls are perpendicular and thus make it possible to preserve the cubic structure. However, the rotation of the phenyl groups breaks the conjugation path of the π electrons and therefore each ring can be considered as separate in terms of aromaticity.

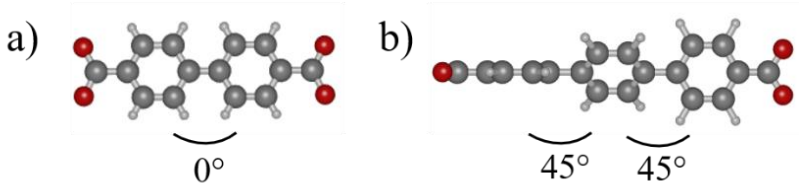

Figure 4. Torsion angles of a) BPDC and b) TPDC. Carbon: grey, oxygen: red and hydrogen: white.

In the case of cyclohexane, the elongation of BDC to BPDC is beneficial as K_H values show (+28%). Counter to the rigid benzene, cyclohexane due to its flexibility can accommodate more efficiently and interact with multiple benzene rings without elevated steric constraints. It also appears that this positive effect disappears gradually when ligand is too long due to a loss of interactions with the MOF walls.

Keeping these structural differences in mind, at this point it can be stated that *i)* for benzene, a decrease in K_H value for IRMOF-10 (-52 % vs IRMOF-1) is mainly due to a loss of interaction number caused by the expansion of the unit cell , *ii)* while additional phenyl rings is advantageous for cyclohexane since it increases the number of potential interactions and iii) the slight difference in K_H values between IRMOF-10 and -16 is related to the similar aromatic character of BPDC and TPDC.

On the contrary, IRMOF-14 is composed of a pyrene-based ligand exhibiting a highly symmetrical polyaromatic structure with four fused phenyl rings. Unlike BPDC and TPDC ligands, pyrene has no annulenoid conjugation due to the strong delocalized of π electrons. This particularity has been widely exploited for the design of pyrene-based MOFs used in the context of luminescence detection, (photo)catalysis and gas adsorption/separation[47]. IRMOF-14 shows high improvement of K_H values compared to IRMOF-1 (+290 and +54% for cyclohexane and benzene, respectively). This result suggests that a highly conjugated ligand is beneficial for

increases benzene/cyclohexane affinity. Indeed, the pyrene ligand possessing a high π electron density provides a large surface available for potential host-guest interactions with benzene and cyclohexane. Moreover, the planarity of the ligand allows the efficient accommodation of VOCs in the MOF cavities.

The density plots of benzene and cyclohexane in IRMOF-14 confirm the favorable interactions of both adsorbates, especially with benzene while cyclohexane follows the same behavior as in the case of IRMOF-1 (**Figure 5**). Furthermore, it should be mentioned that the computational results as obtained are well in line with the results obtained elsewhere[29] on another MOF (SION-82) composed of pyrene-based ligands and exhibiting higher affinity by π-π stacking for aromatics such as pyridine, thiophene and benzene.

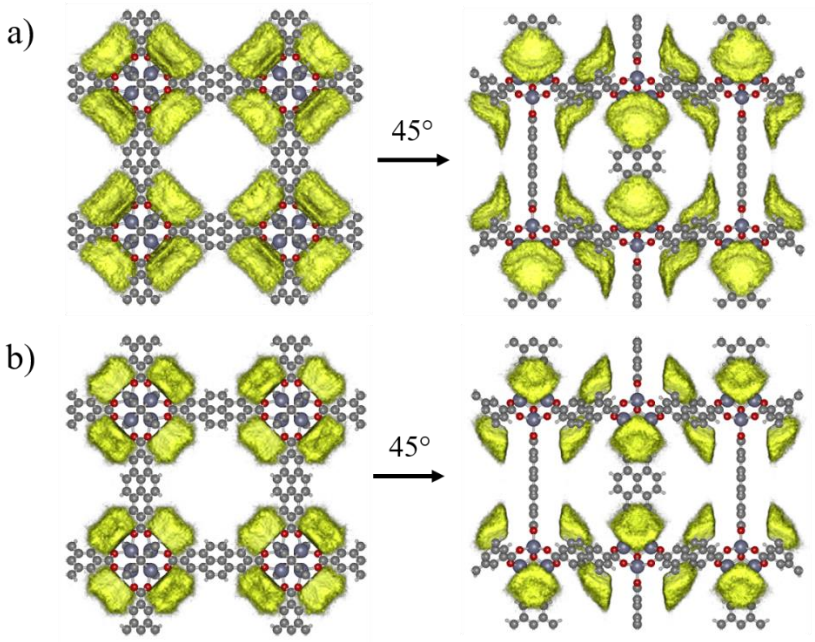

Figure 5. Density plots for a) benzene and b) cyclohexane in IRMOF-14 structure. Zinc: dark grey, carbon: light grey, oxygen: red and hydrogen: white.

Adsorption enthalpies were also estimated for each system using Henry's constant calculated at different temperatures and van't Hoff relation. Regarding IRMOF-1, the ΔH_{ads} values were

estimated at -33.2 and -32.7 kJ/mol for cyclohexane and benzene respectively. The theoretical values reported in the literature for benzene span from -29.19 kJ/mol to -39.37 kJ/mol[32,48,49], while the experimental ones are comprised between -31.8 and -55 kJ/mol[50–52] (**Table 4**). The estimated adsorption enthalpy for benzene in our work thus remain in the same range, comforting the relevance of our calculations. The estimated adsorption enthalpy for benzene in our work thus remain in the same range, comforting the relevance of our calculations. It is to note that the difference between reported theoretical and experimental values can be partly explained by the selected calculation method of adsorption enthalpy. Furthermore, W.-G. Shim et al. highlighted experimentally by using Fowler-Guggenheim local isotherm approach the presence of two different adsorption sites in IRMOF-1 featuring specific values of adsorption enthalpy -31.8 and -40.1 kJ/mol, respectively[51]. The site of lower energy (-31.8 kJ/mol) is largely dominant and covers 7.7 times higher surface than the second one of higher energy (-40.1 kJ/mol). However, their nature still remains unclear. M.T. Luebbers et al.[52] shed some light into this subject by preparing three samples of IRMOF-1 with different specific surface areas (208, 781 and 1161 m^2/g) and their adsorption enthalpy for benzene was determined on the basis of the temperature depending retention using gas chromatography. It has been suggested that the decrease of specific surface area caused by the formation of nonporous degraded phase results in the presence of stronger binding sites and thus an increase of the adsorption enthalpy compared with the structurally perfect IRMOF-1. In a similar way, the general trend presented in our study shows that the calculated value of the adsorption enthalpy for an ideal IRMOF-1 is effectively lower than in defect containing IRMOF-1. Hence, a certain overestimation of the adsorption enthalpy is inevitable between the theoretical and experimental values for real samples. This finding is not surprising, taking into account the low chemical stability of IRMOF-1 undergoing its structure amorphization

under the air atmosphere[17]. This observation is also applicable for cyclohexane. Interestingly, for this adsorbate, the calculated value (-33.2 kJ/mol) is close to the experimental one (-36.25 kJ/mol)[52], while the reported theoretical adsorption enthalpy obtained by DFT is much lower (-42.85 kJ/mol)[32]. As mentioned previously, IRMOF-1 contains two types of cavity (11 and 15 Å), however for DFT calculation of binding energy only one cavity is typically selected. Nevertheless, it could not be guaranteed that both cavities exhibit the same adsorption enthalpy, hence the estimated value by DFT may differ from those obtained by GCMC which takes into account the whole structure. Unfortunately, a comparison with literature for the other IRMOFs remains tricky due to the lack of experiment data on these systems but the confirmation of the validity of our calculated adsorption enthalpies gives strong credibility to those computationally obtained with the same method for the other considered IRMOFs.

Table 4. Reported values of adsorption enthalpies for IRMOF-1 interacting with benzene or cyclohexane.

Reference	Surface Area (m^2/g)	ΔH_{ads} (kJ/mol)	Method
Benzene (Simulation)			
L. Macreadie et al.[32]	3906[53]	-39.37	DFT
F. D. Lahoz-Martín et al.[48]		-29.19	GCMC
Y. Zeng et al.[49]		-37.82 -36.89	GCMC
Benzene (Experiment)			
W. Makowski et al.[50]	679	-55.0	Quasi-equilibrated temperature programmed desorption
W.-G. Shim et al.[51]	2919	-31.8 -40.1	Fowler-Guggenheim local isotherm

M.T. Luebbers et al.[52]	1161	-42.21	Temperature dependence of retention
	781	-46.66	
	208	-51.07	
Our work	**3906**	**-32.7**	**GCMC**
Cyclohexane (Simulation)			
L. Macreadie et al.[32]	3906	-42.85	DFT
Cyclohexane (Experiment)			
M.T. Luebbers et al.[52]	1161	-36.25	Temperature dependence of retention
Our work	**3906**	**-33.2**	**GCMC**

For IRMOF-10, one may observe a slight drop of ΔH_{ads}, especially for the benzene molecule. Since benzene is more affected by the core of the organic ligand than by the environment of the Zn_4O cluster, it can be assumed that the reduction of π electron density in BPDC leads to decrease of ΔH_{ads}. On the other hand, cyclohexane exhibits an opposite behavior and since the environment of the Zn_4O metal center area is not influenced by the presence of organic ligands, it does not have a significant impact on the ΔH_{ads} of this adsorbate. The same conclusion can be drawn for IRMOF-16 in which the ΔH_{ads} of cyclohexane is not significantly impacted. Moreover, there is no significant differences of ΔH_{ads} between IRMOF-10 and -16 exposed to benzene or cyclohexane. This finding can be explained by the availability of C-H bonds induced by phenyl rotation in TPDC. Indeed as this ligand is a C-H···π donor/acceptor like benzene, interactions other than π-π stacking can occur mutually. In the case of IRMOF-14, the variation of ΔH_{ads} is significantly higher. This phenomenon could be explained by the presence of a large aromatic surface which allows higher interactions of benzene and cyclohexane and their better accommodation in the MOF cavities. Moreover, the increase in ΔH_{ads} can also be attributed to higher π electron density

enhancing adsorbate interactions. Therefore, it can be assumed that ligands composed of fused phenyl rings appear to significantly enhance host-guest interactions at low loadings.

Co-adsorption

To assess the adsorption efficiency of IRMOF when exposed to a gas mixture environment, co-adsorption isotherms for an equimolar mixture of benzene and cyclohexane were obtained by GCMC for pressure range from 0.1 to 1.0 kPa at 298K. These simulations showed different behaviors for each MOF studied (**Figure 6**). Cyclohexane is preferentially adsorbed compared to benzene, even at very low pressures for all structures. This observation was confirmed in the literature at least in the case of IRMOF-1 by Macreadie et al.[32] who obtained co-adsorption isotherms using the IAST approach and single-component isotherms[32]. However, some deviations from the reported values can be explained both by the difference of working temperature (298 vs 293 K) but also the errors generated by the necessary hypothesis required for IAST which concerning the chemical similarity of the studied adsorbates[54–56]. However, this assumption could not be applied in the case of benzene (rigid, planar and aromatic) and cyclohexane (flexible, aliphatic with different potential 3D conformations). Indeed, the comparison between the selectivities obtained computationally for IRMOF-1 and those obtained by Macreadie et al. using IAST method[32] shows some differences (Figure S8a). This discrepancy could be explained by *i)* the lack of chemical similarity between adsorbates, *ii)* the quality and the model choice for curve fitting and *iii)* the calculated adsorption enthalpies as discussed previously. The absolute value may thus differ due to the assumptions and uncertainties of IAST methods and the amount of defects in the IRMOF-1 structure, while the trends in selectivity remain qualitatively similar between both experimental and theoretical values.

For the best of our knowledge, no experimental results are reported concerning the co-adsorption of benzene/cyclohexane mixtures for the other isoreticular MOFs and therefore, further comparisons are still limited for these cases. However, one may assume that the fact that GCMC calculations for IRMOF-1 conserve the same trends than in the literature, provides credibility for the other systems. For expanded structures, isotherms show differences. As for IRMOF-1, cyclohexane is the main adsorbate by IRMOF-10. In this case, the great increase of adsorbed amount is observed at higher pressures (~0.6-0.8 kPa). This lower affinity may be imputed to expansion of cavities which reduces the accommodation efficiency and the number of interactions with the walls. Besides, the saturation is not reached in the largest MOF, IRMOF-16 which supposes lesser affinity. This trend is in agreement with the calculated K_H values which may describe the interaction strength. It may be noticed that the amount of cyclohexane at 1.0 kPa is highest for IRMOF-10 (~30 mmol/g vs 14 and 1.2 mmol/g for IRMOF-10, -1 and -16 respectively). It appears that this structure exhibits a trade-off between available pore space and enough host-guest interactions to accommodate molecules. When too large, pores are not capable of being fully filled. Inversely, too small pores are quickly saturated and exhibits limited storage capacity. Interestingly, in the case of IRMOF-14 composed of pyrene groups, one can notice a significant increase in cyclohexane adsorption up to ~25 mmol/g at 1.0 kPa which is almost twice than for IRMOF-1. This observation shows that the elongation of the linker, which has a negative impact on the amount of adsorbed cyclohexane, seems to be counterbalanced by the higher aromaticity of the ligand. These results are in good agreement with the calculated values of K_H. Moreover, the pressure at which the adsorption curves split, is shifted to lower values when BPDC (IRMOF-10) is replaced with PDC (IRMOF-14), both ligands with similar sizes. The comparison of coadsorption isotherms of each selected MOFs shows that pyrene group in IRMOF-14 allows

increasing significantly the affinity toward cyclohexane which is adsorbed at relatively low pressures and offering high adsorption capacity, much higher than for IRMOF-1 which confirms the relevancy to introduce pyrene-containing ligands in MOFs for the industrial separation of cyclohexane/benzene mixtures.

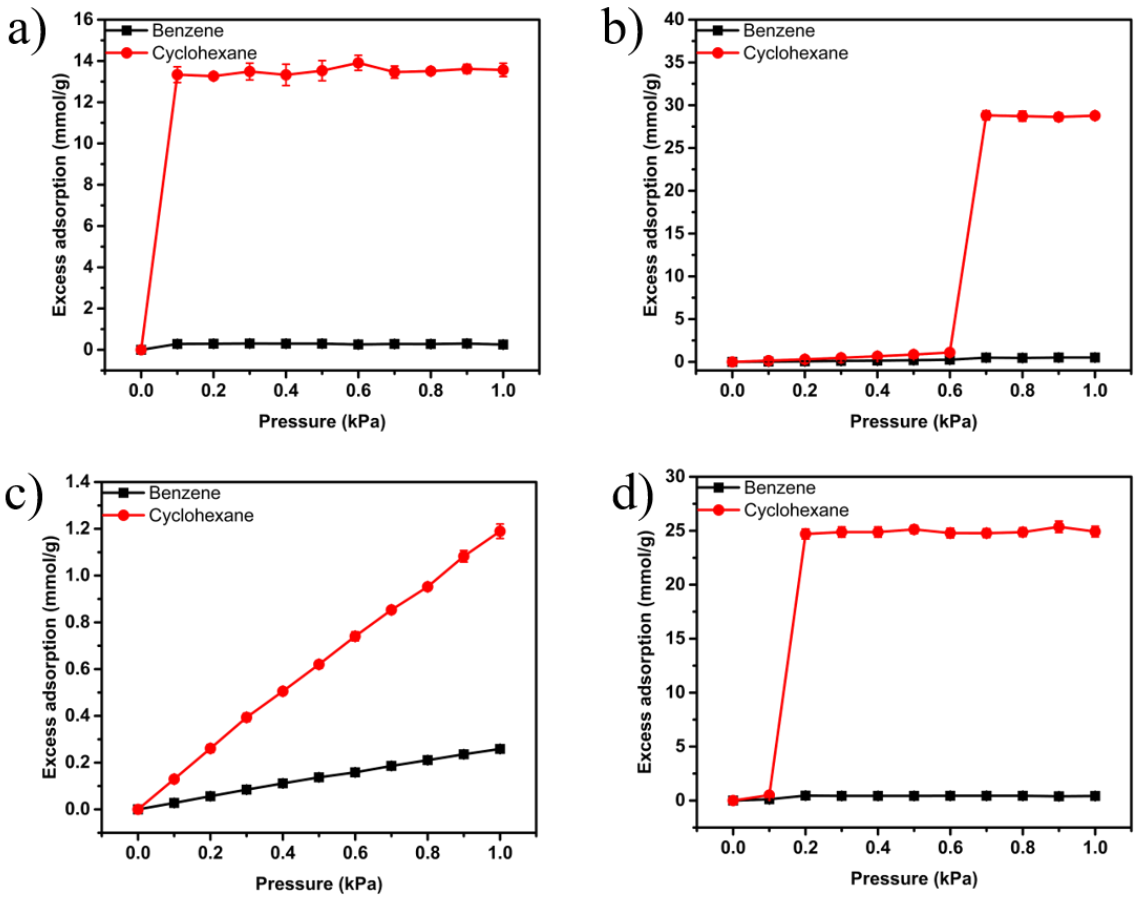

Figure 6. Co-adsorption isotherms at 298K of an equimolar mixture of benzene and cyclohexane for a) IRMOF-1, b) IRMOF-10, c) IRMOF-16 and d) IRMOF-14.

The comparison of selectivity curves for each IRMOF provides additional complementary information on their performance for practical benzene/cyclohexane separation. The results evidence a plateau at 0.025 and 0.22 for IRMOF-1 and IRMOF-16 respectively in a range from 0 to 1 kPa (Figure S8b). IRMOF-16 exhibits one of the highest and constant selectivity for benzene

while IRMOF-1 favors adsorption of cyclohexane. IRMOF-10 and IRMOF-14 do not follow linear trend which was also observed in their coadsorption isotherms. Indeed, a significant drop is present at 0.1-0.2 and 0.6-0.7 kPa for IRMOF-14 and IRMOF-10, respectively. Their initial cyclohexane/benzene selectivity (0.24) decreases to 0.02 for both of them, a value similar to IRMOF-1. IRMOF-14 containing pyrene groups exhibits similar selectivity as IRMOF-1 but its adsorption capacity is almost twice as high. These results demonstrate the benefit of inserting highly aromatic pyrene functional groups in the MOF structure to boost host-guest interactions and thus the uptake capacity of the material.

Conclusion

The impact of ligand aromaticity (contribution of π electrons) on the adsorption efficiency of benzene was investigated in a comparison with its non-aromatic counterpart (cyclohexane). For that purpose, four isoreticular MOFs (IRMOF-1, -10, -14 and -16) were selected. IRMOF-14 was considered due to the presence of ligands containing a pyrene core exhibiting high π electron density, while the other three IRMOFs were composed of separate phenyl rings featuring fewer conjugated ligands. Evaluation of the IRMOF-benzene and IRMOF-cyclohexane systems showed that their K_H values decrease with increasing ligand length. On the other hand, the presence of the pyrene group significantly improves the K_H up to ~290 and 54% for cyclohexane and benzene, respectively. The calculation of the presence density for both adsorbates indicated that cyclohexane is preferentially located near the metal center (Zn_4O clusters) while benzene interacts simultaneously with the metal center and the organic ligand thus showing a favorable impact of the pyrene group on adsorption efficiency. Indeed, adsorption enthalpies were found to be much improved for such fused-aromatic systems indicating enhanced host-guest interactions. The co-adsorption isotherms obtained by the GCMC method showed that the amount of adsorption

decreases with increasing ligand length (IRMOF-10 and -16), although this phenomenon is counterbalanced for IRMOF-14 due to the presence of pyrene group exhibiting a large surface area of adsorption and high π electron density. Interestingly, the slopes of the adsorption isotherm for cyclohexane are shifted towards higher pressures according to this trend: IRMOF-1 < IRMOF-10 < IRMOF-16. This finding can be explained by reduced interactions of adsorbates with the MOF walls within the cavities of IRMOF-10 and -16. However, the negative impact of ligand elongation on the slope location seems to be significantly counterbalanced by high pyrene aromaticity. This study thus highlights the advantage of fused-aromatic ring-based ligands in the MOF structure for the effective removal or detection of dilute harmful hydrocarbons, offering attractive potential for applications in air purification and VOC sensing. Regarding the challenging separation of the azeotropic benzene/cyclohexane mixture, the obtained results demonstrate the great improvement of separation efficiency of pyrene-containing MOFs which may therefore offer another strategy to design high-performing MOFs.

Corresponding Author

* Martin Drobek - Institut Européen des Membranes, UMR 5635, Université de Montpellier, ENSCM, CNRS, Place Eugène Bataillon, F-34095 Montpellier cedex 5, France

Email: martin.drobek@umontpellier.fr

Authors

Kevin Dedecker - Institut Européen des Membranes (IEM); CNRS, ENSCM, Univ Montpellier; Place Eugène Bataillon; 34095 Montpellier; France

Email: kevin.dedecker@umontpellier.fr

Anne Julbe - Institut Européen des Membranes (IEM); CNRS, ENSCM, Univ Montpellier; Place Eugène Bataillon; 34095 Montpellier; France

Email: anne.julbe@umontpellier.fr

Author Contributions

The manuscript was written through contributions of all authors. All authors have given approval to the final version of the manuscript.

Notes

The authors declare no competing financial interest. The funders had no role in the design of the study; in the collection, analyses, or interpretation of data; in the writing of the manuscript; or in the decision to publish the results.

Supporting Information. Model of benzene and cyclohexane, equilibration for calculation of K_H and coadsorption, estimation of adsorption enthalpy, density plot of IRMOF-10 and IRMOF-16, selectivity curves of IRMOFs.

ACKNOWLEDGMENT

This research was funded by the ANR SensMOFAir project (#ANR-20-CE04-0012).

REFERENCES

(1) Khan, F. I.; Kr. Ghoshal, A. Removal of Volatile Organic Compounds from Polluted Air. *J. Loss Prev. Process Ind.* **2000**, *13* (6), 527–545. https://doi.org/10.1016/S0950-4230(00)00007-3.

(2) Carslaw, N.; Creasey, D. J.; Harrison, D.; Heard, D. E.; Hunter, M. C.; Jacobs, P. J.; Jenkin, M. E.; Lee, J. D.; Lewis, A. C.; Pilling, M. J. et al. OH and HO2 Radical Chemistry in a

Forested Region of North-Western Greece. *Atmos. Environ.* **2001**, *35* (27), 4725–4737. https://doi.org/10.1016/S1352-2310(01)00089-9.

(3) Wang, Q.; Han, Z.; Wang, T.; Zhang, R. Impacts of Biogenic Emissions of VOC and NOx on Tropospheric Ozone during Summertime in Eastern China. *Sci. Total Environ.* **2008**, *395* (1), 41–49. https://doi.org/10.1016/j.scitotenv.2008.01.059.

(4) Carter, W. P. L. Development of Ozone Reactivity Scales for Volatile Organic Compounds. *J. Air Waste Manag. Assoc.* **1994**, *44* (7), 881–899. https://doi.org/10.1080/1073161x.1994.10467290.

(5) Li, A. J.; Pal, V. K.; Kannan, K. A Review of Environmental Occurrence, Toxicity, Biotransformation and Biomonitoring of Volatile Organic Compounds. *Environ. Chem. Ecotoxicol.* **2021**, *3*, 91–116. https://doi.org/10.1016/j.enceco.2021.01.001.

(6) Sharma, N.; Agarwal, A. K.; Eastwood, P.; Gupta, T. *Air Pollution and Control*, 1st ed.; Sharma, N., Agarwal, A. K., Eastwood, P., Gupta, T., Singh, A. P., Eds.; Energy, Environment, and Sustainability; Springer Singapore: Singapore, 2018. https://doi.org/10.1007/978-981-10-7185-0.

(7) Cheng, S.; Zhang, J.; Wang, Y.; Zhang, D.; Teng, G.; Chang-Chien, G. P.; Huang, Q.; Zhang, Y. B.; Yan, P. Global Research Trends in Health Effects of Volatile Organic Compounds during the Last 16 Years: A Bibliometric Analysis. *Aerosol Air Qual. Res.* **2019**, *19* (8), 1834–1843. https://doi.org/10.4209/aaqr.2019.06.0327.

(8) Montero-Montoya, R.; López-Vargas, R.; Arellano-Aguilar, O. Volatile Organic Compounds in Air: Sources, Distribution, Exposure and Associated Illnesses in Children.

Annals of Global Health. Levy Library Press 2018, pp 225–238. https://doi.org/10.29024/aogh.910.

(9) Belingheri, M.; Fustinoni, S.; De Vito, G.; Porro, A.; Riva, M. A. Benzene and Leukemia: From Scientific Evidence to Regulations. A Historical Example. *Med. Lav.* **2019**, *110* (3), 234–240. https://doi.org/10.23749/mdl.v110i3.7995.

(10) Ifeanyi, O. E. A Review on Bezene and Haematological System. *Blood Res. Transfus. J.* **2018**, *2* (2), 1–5. https://doi.org/10.19080/OABTJ.2018.02.555582.

(11) Smith, M. T. Advances in Understanding Benzene Health Effects and Susceptibility. *Annu. Rev. Public Health* **2010**, *31* (1), 133–148. https://doi.org/10.1146/annurev.publhealth.012809.103646.

(12) Roma-Torres, J.; Teixeira, J. P.; Silva, S.; Laffon, B.; Cunha, L. M.; Méndez, J.; Mayan, O. Evaluation of Genotoxicity in a Group of Workers from a Petroleum Refinery Aromatics Plant. *Mutat. Res. - Genet. Toxicol. Environ. Mutagen.* **2006**, *604* (1–2), 19–27. https://doi.org/10.1016/j.mrgentox.2005.12.005.

(13) Cocheo, V.; Sacco, P.; Boaretto, C.; De Saeger, E.; Perez Ballesta, P.; Skov, H.; Goelen, E.; Gonzalez, N.; Baeza Caracena, A. Urban Benzene and Population Exposure. *Nature* **2000**, *404* (6774), 141–142. https://doi.org/10.1038/35004651.

(14) Campos-Ordonez, T.; Gonzalez-Perez, O. Cyclohexane, a Potential Drug of Abuse with Pernicious Effects on the Brain. *Front. Pharmacol.* **2016**, *6,* 1–3. https://doi.org/10.3389/fphar.2015.00291.

(15) Bandosz, T. J. Removal of Inorganic Gases and VOCS on Activated Carbons. In *Adsorption*

by Carbons; Elsevier, 2008; pp 533–564. https://doi.org/10.1016/B978-008044464-2.50025-0.

(16) Marcus, B. K.; Cormier, W. E. Going Green with Zeolites. *Chem. Eng. Prog.* **1999**, *95* (6), 47–52.

(17) Ming, Y.; Purewal, J.; Yang, J.; Xu, C.; Soltis, R.; Warner, J.; Veenstra, M.; Gaab, M.; Müller, U.; Siegel, D. J. Kinetic Stability of MOF-5 in Humid Environments: Impact of Powder Densification, Humidity Level, and Exposure Time. *Langmuir* **2015**, *31* (17), 4988–4995. https://doi.org/10.1021/acs.langmuir.5b00833.

(18) Li, C.; Chandresh, A.; Zhang, Z.; Moulai, S.; Heinke, L. Stability and Degradation of Metal–Organic-Framework Films under Ambient Air Explored by Uptake and Diffusion Experiments. *Adv. Mater. Interfaces* **2022**, *9* (3). https://doi.org/10.1002/admi.202101947.

(19) Yao, H.; Wang, Y.; Quan, M.; Farooq, M. U.; Yang, L.; Jiang, W. Adsorptive Separation of Benzene, Cyclohexene, and Cyclohexane by Amorphous Nonporous Amide Naphthotube Solids. *Angew. Chemie Int. Ed.* **2020**, *59* (45), 19945–19950. https://doi.org/10.1002/anie.202009436.

(20) Ayuso, M.; Cañada-Barcala, A.; Larriba, M.; Navarro, P.; Delgado-Mellado, N.; García, J.; Rodríguez, F. Enhanced Separation of Benzene and Cyclohexane by Homogeneous Extractive Distillation Using Ionic Liquids as Entrainers. *Sep. Purif. Technol.* **2020**, *240*, 116583. https://doi.org/10.1016/j.seppur.2020.116583.

(21) Lu, W.; Wei, Z.; Gu, Z. Y.; Liu, T. F.; Park, J.; Park, J.; Tian, J.; Zhang, M.; Zhang, Q.; Gentle, T. et al. Tuning the Structure and Function of Metal-Organic Frameworks via Linker

Design. *Chem. Soc. Rev.* **2014**, *43* (16), 5561–5593. https://doi.org/10.1039/c4cs00003j.

(22) Zhang, X.; Chen, Z.; Liu, X.; Hanna, S. L.; Wang, X.; Taheri-Ledari, R.; Maleki, A.; Li, P.; Farha, O. K. A Historical Overview of the Activation and Porosity of Metal–Organic Frameworks. *Chem. Soc. Rev.* **2020**, *49* (20), 7406–7427. https://doi.org/10.1039/D0CS00997K.

(23) Dedecker, K.; Dumas, E.; Lavédrine, B.; Steunou, N.; Serre, C. 5 - Metal-Organic Frameworks for the Capture of Volatile Organic Compounds and Toxic Chemicals. In *Metal-Organic Frameworks (MOFs) for Environmental Applications*; Elsevier, 2019; pp 141–178. https://doi.org/10.1016/B978-0-12-814633-0.00007-7.

(24) Dedecker, K.; Drobek, M.; Rouessac, V.; Julbe, A. A Palladium-Based MOF for the Preferential Sorption of Benzene. *ACS Appl. Mater. Interfaces* **2023**, *15* (5), 6831–6838. https://doi.org/10.1021/acsami.2c20034.

(25) Pires, J.; Fernandes, J.; Dedecker, K.; Gomes, J. R. B.; Pérez-Sánchez, G.; Nouar, F.; Serre, C.; Pinto, M. L. Enhancement of Ethane Selectivity in Ethane-Ethylene Mixtures by Perfluoro Groups in Zr-Based Metal-Organic Frameworks. *ACS Appl. Mater. Interfaces* **2019**, *11* (30), 27410–27421. https://doi.org/10.1021/acsami.9b07115.

(26) Dedecker, K.; Pillai, R. S.; Nouar, F.; Pires, J.; Steunou, N.; Dumas, E.; Maurin, G.; Serre, C.; Pinto, M. L. Metal-Organic Frameworks for Cultural Heritage Preservation: The Case of Acetic Acid Removal. *ACS Appl. Mater. Interfaces* **2018**, *10* (16), 13886–13894. https://doi.org/10.1021/acsami.8b02930.

(27) Dasgupta, S.; Biswas, S.; Dedecker, K.; Dumas, E.; Menguy, N.; Berini, B.; Lavedrine, B.;

Serre, C.; Boissière, C.; Steunou, N. In Operando Spectroscopic Ellipsometry Investigation of MOF Thin Films for the Selective Capture of Acetic Acid. *ACS Appl. Mater. Interfaces* **2023**, *15* (4), 6069–6078. https://doi.org/10.1021/acsami.2c17682.

(28) Drobek, M.; Kim, J. H.; Bechelany, M.; Vallicari, C.; Julbe, A.; Kim, S. S. MOF-Based Membrane Encapsulated ZnO Nanowires for Enhanced Gas Sensor Selectivity. *ACS Appl. Mater. Interfaces* **2016**, *8* (13), 8323–8328. https://doi.org/10.1021/acsami.5b12062.

(29) Sudan, S.; Gładysiak, A.; Valizadeh, B.; Lee, J.-H.; Stylianou, K. C. Sustainable Capture of Aromatic Volatile Organic Compounds by a Pyrene-Based Metal–Organic Framework under Humid Conditions. *Inorg. Chem.* **2020**, *59* (13), 9029–9036. https://doi.org/10.1021/acs.inorgchem.0c00883.

(30) He, T.; Kong, X.-J.; Bian, Z.-X.; Zhang, Y.-Z.; Si, G.-R.; Xie, L.-H.; Wu, X.-Q.; Huang, H.; Chang, Z.; Bu, X.-H.; Zaworotko, M. J. et al. Trace Removal of Benzene Vapour Using Double-Walled Metal–Dipyrazolate Frameworks. *Nat. Mater.* **2022**, *21* (6), 689–695. https://doi.org/10.1038/s41563-022-01237-x.

(31) Eddaoudi, M.; Kim, J.; Rosi, N.; Vodak, D.; Wachter, J.; O'Keeffe, M.; Yaghi, O. M. Systematic Design of Pore Size and Functionality in Isoreticular MOFs and Their Application in Methane Storage. *Science (80-.).* **2002**, *295* (5554), 469–472. https://doi.org/10.1126/science.1067208.

(32) Macreadie, L. K.; Qazvini, O. T.; Babarao, R. Reversing Benzene/Cyclohexane Selectivity through Varying Supramolecular Interactions Using Aliphatic, Isoreticular MOFs. *ACS Appl. Mater. Interfaces* **2021**, *13* (26), 30885–30890. https://doi.org/10.1021/acsami.1c08823.

(33) Rai, N.; Siepmann, J. I. Transferable Potentials for Phase Equilibria. 9. Explicit Hydrogen Description of Benzene and Five-Membered and Six-Membered Heterocyclic Aromatic Compounds. *J. Phys. Chem. B* **2007**, *111* (36), 10790–10799. https://doi.org/10.1021/jp0735861.

(34) Rai, N.; Siepmann, J. I. Transferable Potentials for Phase Equilibria. 10. Explicit-Hydrogen Description of Substituted Benzenes and Polycyclic Aromatic Compounds. *J. Phys. Chem. B* **2013**, *117* (1), 273–288. https://doi.org/10.1021/jp307328x.

(35) Muñoz-Muñoz, Y. M.; Guevara-Carrion, G.; Llano-Restrepo, M.; Vrabec, J. Lennard-Jones Force Field Parameters for Cyclic Alkanes from Cyclopropane to Cyclohexane. *Fluid Phase Equilib.* **2015**, *404*, 150–160. https://doi.org/10.1016/j.fluid.2015.06.033.

(36) T.W., G. S.; C.B., F. *Organic Chemistry*, 10th ed.; John Wiley & Sons, Ed.; Hoboken: NJ, 2011.

(37) Sławek, A.; Grzybowska, K.; Vicent-Luna, J. M.; Makowski, W.; Calero, S. Adsorption of Cyclohexane in Pure Silica Zeolites: High-Throughput Computational Screening Validated by Experimental Data. *ChemPhysChem* **2018**, *19* (24), 3364–3371. https://doi.org/10.1002/cphc.201800968.

(38) Li, H.; Eddaoudi, M.; O'Keeffe, M.; Yaghi, O. M. Design and Synthesis of an Exceptionally Stable and Highly Porous Metal-Organic Framework. *Nature* **1999**, *402* (6759), 276–279. https://doi.org/10.1038/46248.

(39) Mayo, S. L.; Olafson, B. D.; Goddard, W. A. DREIDING: A Generic Force Field for Molecular Simulations. *J. Phys. Chem.* **1990**, *94* (26), 8897–8909.

https://doi.org/10.1021/j100389a010.

(40) Rappé, A. K.; Casewit, C. J.; Colwell, K. S.; Goddard, W. A.; Skiff, W. M. UFF, a Full Periodic Table Force Field for Molecular Mechanics and Molecular Dynamics Simulations. *J. Am. Chem. Soc.* **1992**, *114* (25), 10024–10035. https://doi.org/10.1021/ja00051a040.

(41) Yang, Q.; Zhong, C.; Chen, J.-F. Computational Study of CO 2 Storage in Metal−Organic Frameworks. *J. Phys. Chem. C* **2008**, *112* (5), 1562–1569. https://doi.org/10.1021/jp077387d.

(42) Khalil, I.; Jabraoui, H.; Maurin, G.; Lebègue, S.; Badawi, M.; Thomas, K.; Maugé, F. Selective Capture of Phenol from Biofuel Using Protonated Faujasite Zeolites with Different Si/Al Ratios. *J. Phys. Chem. C* **2018**, *122* (46), 26419–26429. https://doi.org/10.1021/acs.jpcc.8b07875.

(43) Wang, G.-D.; Li, Y.-Z.; Shi, W.-J.; Hou, L.; Zhu, Z.; Wang, Y.-Y. A New Honeycomb Metal–Carboxylate-Tetrazolate Framework with Multiple Functions for CO 2 Conversion and Selective Capture of C 2 H 2 , CO 2 and Benzene. *Inorg. Chem. Front.* **2020**, *7* (9), 1957–1964. https://doi.org/10.1039/D0QI00181C.

(44) Pang, J.; Jiang, F.; Wu, M.; Liu, C.; Su, K.; Lu, W.; Yuan, D.; Hong, M. A Porous Metal-Organic Framework with Ultrahigh Acetylene Uptake Capacity under Ambient Conditions. *Nat. Commun.* **2015**, *6* (1), 7575. https://doi.org/10.1038/ncomms8575.

(45) Wang, H.; Qu, Z.; Zhang, W.; Tao, W. Effective Thermal Conductivity of MOF-5 Powder under a Hydrogen Atmosphere. *Computation* **2015**, *3* (4), 558–573. https://doi.org/10.3390/computation3040558.

(46) Jia, J.; Wu, H.-S.; Chen, Z.; Mo, Y. Elucidation of the Forces Governing the Stereochemistry of Biphenyl. *European J. Org. Chem.* **2013**, *2013* (3), 611–616. https://doi.org/10.1002/ejoc.201201273.

(47) Kinik, F. P.; Ortega-Guerrero, A.; Ongari, D.; Ireland, C. P.; Smit, B. Pyrene-Based Metal Organic Frameworks: From Synthesis to Applications. *Chem. Soc. Rev.* **2021**, *50* (5), 3143–3177. https://doi.org/10.1039/D0CS00424C.

(48) Lahoz-Martín, F. D.; Martín-Calvo, A.; Calero, S. Selective Separation of BTEX Mixtures Using Metal–Organic Frameworks. *J. Phys. Chem. C* **2014**, *118* (24), 13126–13136. https://doi.org/10.1021/jp411697z.

(49) Zeng, Y.; Zhu, X.; Yuan, Y.; Zhang, X.; Ju, S. Molecular Simulations for Adsorption and Separation of Thiophene and Benzene in Cu-BTC and IRMOF-1 Metal–Organic Frameworks. *Sep. Purif. Technol.* **2012**, *95*, 149–156. https://doi.org/10.1016/j.seppur.2012.04.032.

(50) Makowski, W.; Mańko, M.; Zabierowski, P.; Mlekodaj, K.; Majda, D.; Szklarzewicz, J.; Łasocha, W. Unusual Adsorption Behavior of Volatile Hydrocarbons on MOF-5 Studied Using Thermodesorption Methods. *Thermochim. Acta* **2014**, *587*, 1–10. https://doi.org/10.1016/j.tca.2014.04.016.

(51) Shim, W.-G.; Hwang, K.-J.; Chung, J.-T.; Baek, Y.-S.; Yoo, S.-J.; Kim, S.-C.; Moon, H.; Lee, J.-W. Adsorption and Thermodesorption Characteristics of Benzene in Nanoporous Metal Organic Framework MOF-5. *Adv. Powder Technol.* **2012**, *23* (5), 615–619. https://doi.org/10.1016/j.apt.2011.07.002.

(52) Luebbers, M. T.; Wu, T.; Shen, L.; Masel, R. I. Trends in the Adsorption of Volatile Organic Compounds in a Large-Pore Metal−Organic Framework, IRMOF-1. *Langmuir* **2010**, *26* (13), 11319–11329. https://doi.org/10.1021/la100635r.

(53) Camp, J.; Stavila, V.; Allendorf, M. D.; Prendergast, D.; Haranczyk, M. Critical Factors in Computational Characterization of Hydrogen Storage in Metal–Organic Frameworks. *J. Phys. Chem. C* **2018**, *122* (33), 18957–18967. https://doi.org/10.1021/acs.jpcc.8b04021.

(54) Cessford, N. F.; Seaton, N. A.; Düren, T. Evaluation of Ideal Adsorbed Solution Theory as a Tool for the Design of Metal–Organic Framework Materials. *Ind. Eng. Chem. Res.* **2012**, *51* (13), 4911–4921. https://doi.org/10.1021/ie202219w.

(55) Kundu, A.; Sillar, K.; Sauer, J. Predicting Adsorption Selectivities from Pure Gas Isotherms for Gas Mixtures in Metal–Organic Frameworks. *Chem. Sci.* **2020**, *11* (3), 643–655. https://doi.org/10.1039/C9SC03008E.

(56) Chen, H.; Sholl, D. S. Examining the Accuracy of Ideal Adsorbed Solution Theory without Curve-Fitting Using Transition Matrix Monte Carlo Simulations. *Langmuir* **2007**, *23* (11), 6431–6437. https://doi.org/10.1021/la700351c.